

Negative-permeability electromagnetically induced transparent and magnetically active metamaterials

K. L. Tsakmakidis,¹ M. S. Wartak,^{2,1} J. J. H. Cook,¹ J. M. Hamm,¹ and O. Hess^{1,*}

¹*Advanced Technology Institute and Department of Physics, Faculty of Engineering and Physical Sciences, University of Surrey, Guildford GU2 7XH, United Kingdom*

²*Department of Physics and Computer Science, Wilfrid Laurier University, Waterloo, Ontario, Canada N2L 3C5*

(Received 31 January 2010; revised manuscript received 28 March 2010; published 27 May 2010)

Metamaterials exhibiting *negative* electromagnetic parameters can enable a multitude of exciting applications, but currently their performance is limited by the occurrence of losses—particularly *radiation* losses, which dominate over their dissipative counterparts even in the optical regime. Here, a metamaterial configuration is conceived that judiciously *generalizes* the traditional electromagnetically induced transparency (EIT) scheme—by which radiation losses can be restrained—in such a way that EIT can be observed and exploited in negative-magnetic metamaterials. Analytic theory and three-dimensional simulations unveil the required route: introduction of *poor*-conductor meta-atoms next to the good-conductor meta-atoms of a magnetic metamaterial. This setup results in a frequency band where the metamaterial remains negative-magnetic, while its loss-performance dramatically *improves* owing to suppression of radiation damping. Furthermore, we show that placing the two meta-atoms on orthogonal planes gives rise to a passive anisotropic metamaterial exhibiting permeabilities with negative real parts ($\text{Re}\{\mu\} < 0$) and *active* imaginary parts ($\text{Im}\{\mu\} > 0$ for an $e^{+i\omega t}$ time dependence) along its principal crystallographic axes.

DOI: [10.1103/PhysRevB.81.195128](https://doi.org/10.1103/PhysRevB.81.195128)

PACS number(s): 78.67.Pt, 42.25.Bs, 42.25.Fx, 78.20.Ci

I. INTRODUCTION

Macroscopic composite materials exhibiting unusual electromagnetic properties, known as metamaterials (MMs), have recently been fabricated, tested and were shown to be in good agreement with theory all the way from the radio¹ up to the optical² regime. These materials allow for the realization of a plethora of electromagnetic phenomena and devices, unattainable using natural materials, such as “perfect” lenses,³ “invisibility” cloaks,⁴ optical circuits and antennas,⁵ and broadband deceleration and stopping of light.⁶ To allow for such functionalities, use is made of engineered “metamolecules” whose electromagnetic parameters (effective permeability μ and permittivity ϵ) can be tailored to enter highly unusual regimes, such as one where ϵ and μ are simultaneously negative, leading to a negative effective refractive index n (Ref. 7). However, at present the performance of metamaterials is limited by the occurrence of losses, which occasionally can be up to tens of dB/wavelength (Ref. 8). Although a number of possible routes toward overcoming this problem have been proposed, these solutions, so far, either cannot be deployed at specific frequency regimes of interest (e.g., at the THz regime), or result in the metamaterial not maintaining the negativity in the real part of its constitutive parameters.

The losses that occur in present-day metamaterials have two primary components: radiation and dissipation—with the first component far exceeding the second one.^{9–11} Radiation losses^{9–11} originate from the part of the incident wave that is (temporarily) imparted on each meta-atom, but then reradiated (scattered) off by the resultant oscillating charges and currents in a direction not necessarily the same as the one followed by the primary wave; see Fig. 1. This part of the incident wave that is reradiated/scattered (by each meta-atom) *away* from the primary transmitted wave counts as a

source of loss, affecting adversely the loss-behavior of the metamaterial. The second component of losses arises from intrinsic metallic/dissipative losses, which are ohmic in nature and are associated with photon absorption. Unfortunately, it turns out that for metamaterials, radiation losses are much greater than their ohmic counterparts, *even in the optical regime*,⁹ i.e., in the regime where the ohmic losses are high. Furthermore, even when use is made of *purely dielectric* (i.e., not metallic) meta-atoms to mitigate the intrinsic metallic/ohmic losses, the obtained magnetic susceptibilities

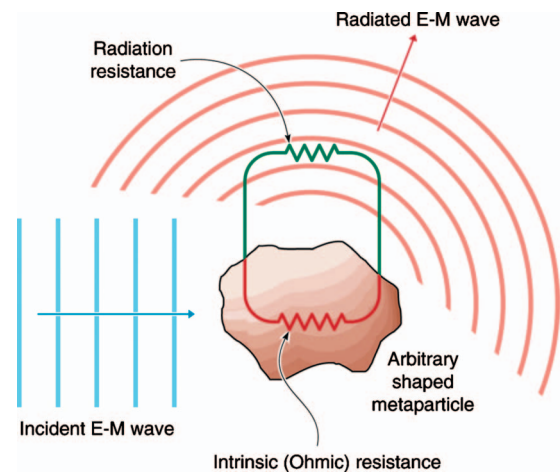


FIG. 1. (Color) Origin of losses in metamaterials. An incident electromagnetic wave impinges on a metaparticle (e.g., a split-ring resonator). Part of the wave localizes inside the metaparticle and is eventually converted (lost) into heat through an equivalent intrinsic/ohmic resistance. A much larger part of the incident wave is radiated/scattered off the metaparticle, contributing to the, so-called, radiation losses of the particle via an equivalent “radiation resistance.”

do still have a (relatively) large imaginary part (see below), leading to “figures-of-merit” that remain at the order of only 1–10 (Ref. 12)—similar to their metallic counterparts. This detrimental role of radiation losses in shaping the loss-behavior of metamaterials has, by now, been clearly and convincingly pointed out.^{9–11} However, a *solution* to this problem—in a regime where a metamaterial *preserves* its negative parameters—has remained elusive. If such a solution could be found, then up to the THz regime we would be able to harness practically “*lossless*” negative-parameters metamaterials with dramatically enhanced figures-of-merit, since metals in these regimes are almost perfect conductors, expelling electromagnetic fields from their interior. Indeed, a very similar situation (again up to THz frequencies) also occurs, e.g., for “spoof” surface plasmons (SPs), for which the intrinsic metallic losses are (almost) not an issue^{13,14}—and one is primarily concerned with the spoof SPs’ spatial extension and confinement, rather than their dissipation.

So far, a number of diverse strategies have been proposed toward overcoming the issue of high losses in metamaterials.¹⁵ A first approach relies on the use of stimulated emission to compensate the overall metamaterial losses.¹⁶ This approach is very promising and it has, in fact, been theoretically predicted that it can lead to zero-loss metamaterials, even over a broad yet finite bandwidth.¹⁷ However, it may not always be possible to find a suitable medium to provide the necessary gain at a desired frequency regime. Further, such a strategy is not particularly well-suited for confronting the *primary* component of metamaterial losses (that has a geometric/design origin, rather than an ohmic one), and if deployed it may result in *increasing* the radiation losses—although the ohmic or overall losses are, indeed, expected to decrease or be completely eliminated. It is also to be noted that use of stimulated emission for mitigating losses gives invariably rise to amplified spontaneous emission *noise*, which deteriorates the signal-to-noise ratio (SNR)—an extremely important figure-of-merit for, e.g., optical communication systems.

A second interesting strategy makes use of negatively reflecting/refractive interfaces to reproduce the features of bulk negative-index metamaterials.¹⁸ Upon being negatively refracted at the engineered interfaces, light is allowed to propagate through lossless dielectric materials, such as air, thereby avoiding high-attenuation regions. This scheme relies on the use of nonlinear media and therefore requires intense incident light, which may give rise to nonlinear absorption effects, such as two-photon absorption and amplified spontaneous emission.

More recently, a series of works have deployed concepts such as electromagnetically induced or coupled-resonator-induced transparency (EIT/CRIT) (Ref. 19) to overcome metamaterial losses.^{20–26} Unfortunately, although in these metamaterial EIT/CRIT-analogs radiation losses *are* substantially suppressed, this is performed in a regime where the metamaterial’s effective parameters (permittivity, ϵ , permeability, μ , refractive index, n) do *not* preserve the negativity in the responses of their real parts.^{22,24,25} Essentially, this is because the adherence of these schemes to a strict EIT/CRIT-analog, results in the radiation losses being reduced at^{20–23,25,26} or below²⁴ the main resonance, i.e., in a regime

where the real parts of the medium’s constitutive parameters are invariably non-negative—similarly to EIT or CRIT. Thus, although such *diamagnetic* metamaterials are expected to find interesting applications in their own right, e.g., in enabling enhanced biomolecular sensing^{23,24} or diamagnetic levitation, unfortunately they cannot be used in a multitude of exciting and intriguing *negative-parameters* based metamaterial applications, such as subwavelength focusing,³ *negative-index* based invisibility or “illusion” media,²⁷ metamaterial-inspired optical nanocircuits (“metacronics”) (Ref. 5), “trapped rainbow”-slowing and stopping of light,⁶ and so forth. Note that obtaining low-loss electromagnetic parameters with negative real parts has the important additional advantage that we can also eliminate *reflection* losses, since with such media one can achieve a *perfect impedance matching* to, both, positive-index *bulk* media³ and *waveguides*.⁶

It is the objective of this work to introduce a suitable metamaterial configuration that allows for the attainment of suppressed, EIT-enabled, radiation losses *outside* the first quadrant ($\epsilon > 0$ and $\mu > 0$) of the “ ϵ - μ plane”—in a regime where negative-parameters ($\epsilon < 0$ and/or $\mu < 0$) metamaterials can profit. We show that such a dramatically enhanced metamaterial loss-behavior is not achieved by attempting to further improve the conductivity of the metamaterial’s “atoms” [split-ring resonators, (SRRs)], but instead by placing poor-conductor SRR (p-SRR) meta-atoms next to the existing good-conductor SRR (g-SRR) meta-atoms of the magnetic metamaterial—an arrangement that, as is shown in the following, results in suppression of radiation damping associated with the existing g-SRR atoms of the metamaterial.

The organization of the paper is the following. Section II is devoted to a closer examination of the loss mechanisms in isolated and paired SRR meta-atoms. An analytic treatment indicates that a suitably designed pair of SRR meta-atoms exhibits almost totally suppressed radiation losses; its loss-behavior being limited only by the inherent dissipative losses of its metallic constituents (with these losses being extremely small for frequencies up to the THz regime). A three-dimensional finite-element analysis of the absorption spectra of such a pair of SRRs (designed according to the aforementioned analytic recipe) is found to be in excellent agreement with the theoretical model, confirming the attainment of dramatically reduced radiation losses. In Sec. III, it is shown that when the afore-studied SRRs are placed on orthogonal planes, a magnetically anisotropic metamaterial emerges, which exhibits *active* permeabilities (μ) along its crystallographic axes (for the assumed $e^{i\omega t}$ time-dependence, this means: $\text{Im}\{\mu\} > 0$). We study the dispersion relations characterizing this metamaterial, and we show that despite the fact that it can be designed such that it is nonbianisotropic and magnetically active (with $\text{Re}\{\mu\} < 0$), the refractive index (n) of an eigenwave propagating through it, is always passive ($\text{Im}\{n\} < 0$) and positive ($\text{Re}\{n\} > 0$). Section IV shows that the described mechanism for suppressing radiation losses or observing (anisotropic) magnetically active behavior, is robust to the presence of even strong dissipative losses; hence, it can, in principle, be extended to optical frequencies. Finally, Sec. V summarizes the paper presenting the main conclusions of the present study.

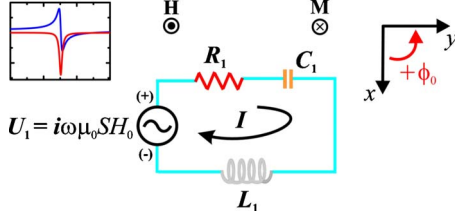


FIG. 2. (Color online) Equivalent circuit model describing the effective- μ behavior of a split-ring resonator (SRR). Here, it is assumed that the magnetic metaparticle is *nonbianisotropic*, characterized by an effective permittivity $\epsilon=1+i0$. One may, also, use real lumped elements, such as resistors, capacitors and inductors (instead of a physical SRR metaparticle) to obtain the same magnetic responses. The top left inset illustrates a typical variation with frequency of the real (blue) and imaginary (red) part of this structure's effective μ . The top right inset shows the coordinate system used in the analysis.

II. NEGATIVE-MAGNETIC ELECTROMAGNETICALLY INDUCED TRANSPARENT METAMATERIALS

We start our analysis by considering a periodic arrangement of single SRR meta-atoms.²⁸ Each SRR is designed such that it is *nonbianisotropic*²⁹ (see also Sec. III B later on), and can be accurately described by an equivalent R - L - C electric circuit,^{30–34} as shown in Fig. 2, with: $R_1=R_{\text{tot},1}=R_{\text{rad},1}+R_{\text{ohm},1}$ being the meta-atom's *total* (radiation +ohmic) equivalent lumped resistance, L_1 its equivalent lumped inductance and C_1 its equivalent lumped capacitance. A method for experimentally extracting these effective SRR lumped-element parameters (including the $R_{\text{rad},1}$, $R_{\text{ohm},1}$ components) is detailed in Ref. 9.

Let us assume that the SRR meta-atom has an area S , with a unit vector $\hat{\mathbf{a}}=\mathbf{z}_0$ normal to its surface (\mathbf{z}_0 being the unit vector along the z axis), and is located at the center of a unit cell of volume W , periodically repeated in the transverse directions. The whole structure is excited by a plane wave with magnetic field component $\mathbf{H}=H_0\mathbf{z}_0\exp(i\omega t-i\mathbf{k}\cdot\mathbf{d})$ where \mathbf{k} is the wavevector, \mathbf{d} is the vector along the direction of the wave propagation, ω is the angular frequency and t is the time. Assuming that the incident wavelength is considerably larger compared to the internal periodicity of the structure (effective medium approximation), we may accurately regard the incident field to be uniform throughout the structure.^{32,35,36} Furthermore, in this case, and with SRRs at successive unit cells being stacked up closely together (solenoid approximation), the uniform depolarization magnetic field²⁸ only modifies (reduces) the value of the equivalent inductance L in each unit cell.³² Thus, mere reduction in the value of the actual inductance L of each SRR suffices to incorporate the effect of the depolarization field in the analysis. This is, of course, equivalent to assuming that the actual inductance L of each SRR is slightly larger than the inductance (L_1) that we use herein, so that when the (“depolarizing”) mutual inductance L_M is subtracted from L (Ref. 32), we end up with the present value for the equivalent inductance, L_1 ($L_1=L-L_M$).

Each SRR meta-atom, essentially, behaves as a small nanoantenna, re-emitting the energy imparted on it (see Fig.

1), and characterized by a ‘radiation resistance’, which (from basic antenna theory) can—for a circular SRR of radius r —be calculated as:³⁷ $R_{\text{rad},1}=(\pi/6)(\mu_0/\epsilon_0)^{1/2}(kr)^4$. From Faradays’ law, the electromotive force (emf voltage) induced in the equivalent RLC mesh by the \mathbf{H} field will be: $U_{\text{emf}}=-i\omega\mu_0SH_0$. If I is the induced current circulating the mesh, application of Kirchhoff’s second law in this circuit gives: $U_1=\text{abs}(U_{\text{emf}})=i\omega\mu_0SH_0=I(R_1+i\omega L_1+1/(i\omega C_1))$. Assuming low-density, weakly interacting (“isolated”) unit cells, the last expression, together with the relations: $\mathbf{I}=-I\boldsymbol{\varphi}_0$ and $\mathbf{M}=-m/W\mathbf{z}_0=-(\mu_0IS/W)\mathbf{z}_0$, with $\boldsymbol{\varphi}_0$, m , and \mathbf{M} being the unit polar-angle vector, induced magnetic moment and magnetization, respectively, leads to the following expression for the effective magnetic polarizability: $\alpha_\mu=\omega^2\mu_0^2S^2C_1/[i\omega C_1R_1+(1-\omega^2L_1C_1)]$. Here, the important point for the following is that, unless the radiation re-emitted by each meta-atom is (by some *extrinsic* means) suppressed or cancelled out, the *imaginary* part of α_μ will be *nonzero even* when the SRR meta-atom is intrinsically *lossless*¹¹—a requirement that is stipulated from dispersion-theory considerations³⁶ (based on Larmor’s formula), as well as from the conservation of energy.¹¹ Indeed, using the above expression for $R_{\text{rad},1}$, one finds that *even when* $R_{\text{ohm},1}=0$, it is: $\text{Im}\{1/\alpha_\mu\}=R_{\text{rad},1}/\omega\mu_0^2S^2=k^3/(6\pi\mu_0)$ —*independently* of the meta-atoms’ radius r , i.e., even in the deep-subwavelength regime.

Now, let us consider placing a new (nonbianisotropic) poor-conductor SRR (p-SRR) meta-atom “2” next to *each* existing good-conductor SRR (g-SRR) meta-atom ‘1’ of our initial metamaterial, as shown in Fig. 3(a). The new p-SRR meta-atoms 2 have exactly the same geometrical shape with their neighboring meta-atoms “1” (and therefore: $R_{\text{rad},2}=R_{\text{rad},1}\gg R_{\text{ohm},1}$), but they are made of a much *less* conducting material, such that: $R_{\text{ohm},2}\gg R_{\text{rad},1}$, i.e.: $R_2\gg R_1$. At first glance, it may be thought that such an arrangement will perpetually result in increasing the metamaterial losses, but as we show in the following there is a frequency region where the p-SRR meta-atoms “2” become “invisible” to the incident field, while helping to suppress the radiation scattered off their neighboring g-SRR metaparticles. To see this, let us assume that the previous magnetic field \mathbf{H} is now incident on each *pair* of SRRs, with \mathbf{H} being polarized perpendicularly to the plane of the SRR pair. From Faradays’ law, the electromotive sources (voltages) induced in each pair by the \mathbf{H} field will be: $V_\ell=V_{\text{emf},\ell}=-i\omega\mu_0S_\ell H_0$, $\ell=1,2$, with S_ℓ being the surface of each mesh. If the (experimentally determined) equivalent resistance, inductance and capacitance of the isolated ℓ^{th} meta-atom are, respectively, R_ℓ , L_ℓ , C_ℓ , and C is the capacitance arising from their mutual coupling [see Fig. 3(b)], then the currents circulating in each loop will be given by: $I_\ell=\det(G_\ell)/\det(G)$, where

$$G = \begin{bmatrix} R_1 + i\omega L_1 - i/\omega C_1 - i/\omega C & i/\omega C \\ i/\omega C & R_2 + i\omega L_2 - i/\omega C_2 - i/\omega C \end{bmatrix}, \quad (1a)$$

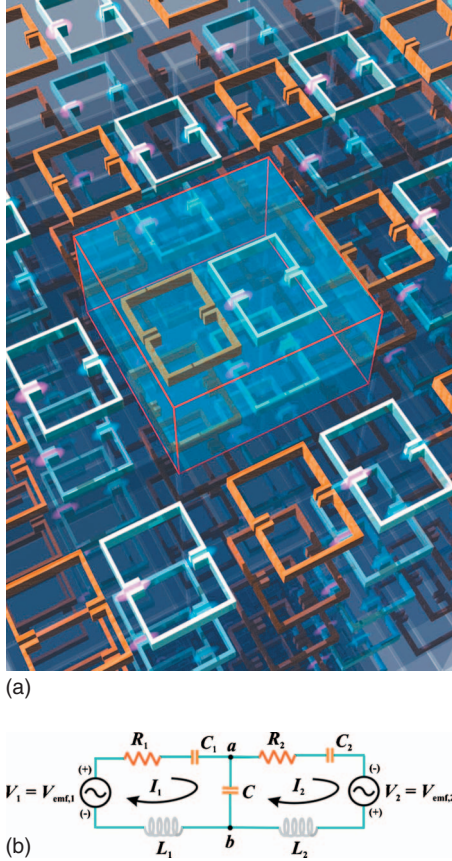


FIG. 3. (Color) (a) Illustration of the design used for obtaining a lossless negative-magnetic metamaterial at GHz frequencies. A poor-conductor SRR (p-SRR) meta-atom (shown in orange) is placed next to each existing good-conductor SRR (g-SRR) meta-atom (shown in white-blue) of a magnetic metamaterial. At a particular frequency, the induced field concentrates solely on the g-SRR particles, with the p-SRR particles neither radiating/scattering off nor dissipating the incident electromagnetic energy. At that frequency, the p-SRR particles only help to induce an accurately antisymmetric mode to each of their g-SRR neighbors—thereby helping to suppress the radiation/scattering damping associated with the g-SRR particles. At the above frequency, only the R_{ohm} component of the g-SRR meta-atoms (which is extremely small at GHz and THz frequencies) contributes to the losses of the metamaterial. Importantly, this enhanced loss-performance occurs in a regime where the metamaterial preserves the negativity in the real of its effective permeability. A unit cell of the magnetic metamaterial is shown as a parallelepiped with red-colored edges. (b) Equivalent circuit model of the pair of the g-SRR meta-atom 1 and p-SRR meta-atom 2 inside the unit cell of the structure shown in (a). The electromotive forces (voltages) V_1 and V_2 are induced by an incident magnetic field that is perpendicular to the areas of the two meta-atoms.

$$G_1 = \begin{bmatrix} V_1 & i/\omega C \\ V_2 & R_2 + i\omega L_2 - i/\omega C_2 - i/\omega C \end{bmatrix},$$

$$G_2 = \begin{bmatrix} R_1 + i\omega L_1 - i/\omega C_1 - i/\omega C & V_1 \\ -i/\omega C & V_2 \end{bmatrix} \quad (1b)$$

with “det” designating the matrix determinant. Having cal-

culated the currents I_ℓ circulating in each mesh, one may determine the magnetization M as the *total* magnetic dipole moment (emanating from *both* meshes) per unit volume, using $M = (S_1 I_1 + S_2 I_2) / W$.

Note that the two SRR meta-atoms have substantially different *intrinsic* resistances and they *both* couple to the incident field [see Fig. 3(b)]—unlike ordinary-EIT based approaches, where the two resonators have identical intrinsic resistances and a “pump” (exciting) beam couples to *only one* resonator.¹⁹ In this manner, as we show in the following, our magnetic metamaterial can exhibit suppressed radiation losses in a frequency regime *above* its main resonance, i.e., in a regime where the real part of its effective permeability (μ) is negative. For this new MM structure and for the case where the areas of the meta-atoms are equal ($S_2 = S_1$), Figs. 4(a)–4(c) report the (new) real and imaginary parts of the metamaterial’s effective μ , the corresponding figure of merit ($\text{FOM} = -\text{Re}\{\mu\} / \text{Im}\{\mu\}$), as well as the individual active powers P_1 , P_2 [$P_\ell = \text{Re}\{V_\ell I_\ell^*\}$; see the Appendix], and the *total* active power, $P = P_1 + P_2$, for the system of the two meta-atoms in each unit cell. We find from Fig. 4(c) that there is a frequency ($f_1 \approx 13.7834$ GHz) where the radiation dissipated at (owing to the $R_{\text{rad},2}$ component) and emitted from (owing to the $R_{\text{rad},2}$ component) the inserted p-SRR meta-atom 2 is completely suppressed [$P_2 = 0$ exactly; see top right inset in Fig. 4(c)]. This frequency where the lossy p-SRR atom remains effectively unexcited (invisible) corresponds (within the present two-loop circuit picture) to the frequency where the radiation emitted from the neighboring meta-atom 1 is, also, suppressed^{21,23,38} ($P_1 = 0$ at $f_2 \approx 13.784$ GHz). Here, since *both* meta-atoms are ‘bright’^{20,26} resonators and the field reradiated (scattered) from one meta-atom is *allowed* to couple to its neighbor, an observation of vanishing P_2 is a most sensitive signature of suppressed radiation losses arising from meta-atom 1.³⁸ Note that at $f = f_1$ each lossy meta-atom 2 is not only prevented from contributing to the loss-behavior of the metamaterial (since $P_2 = 0$), but it is also used as a crucial element in helping to suppress the radiation emitted from its neighboring g-SRR meta-atom 1. Thereby, at $f = f_1$, it can be expected that the loss-performance of the metamaterial will *only* be limited by the intrinsic ohmic resistance of the g-SRR meta-atom 2.

The above analysis is helpful in showing that, with a judicious choice of the effective R - L - C parameters of each SRR particle, there can be a frequency (*above* the main resonance) where the time-averaged active power associated with the p-SRR vanishes ($P_2 = 0$). This occurs because, at that frequency ($f = f_1$), the voltage V_{ab} in the equivalent model of Fig. 3(b) becomes equal (but with *opposite* polarity) to $V_{\text{emf},2}$, thereby leading to $P_2 = 0$. The rather narrow frequency region around 13.7 GHz where $P_2 < 0$ in the top right inset of Fig. 4(c), is where $V_{ab} > V_{\text{emf},2}$, as a result of which the direction of the current in the lossy p-SRR meta-atom 2 is *reversed*. Note that this current-reversal can, upon judicious choice of the effective R - L - C parameters of the SRR particles, indeed be achieved regardless of the number or the actual form of connection between the equivalent elements that are used for describing the mutual coupling between the two meta-atoms [in the common ‘ ab ’ branch in Fig. 3(b)].

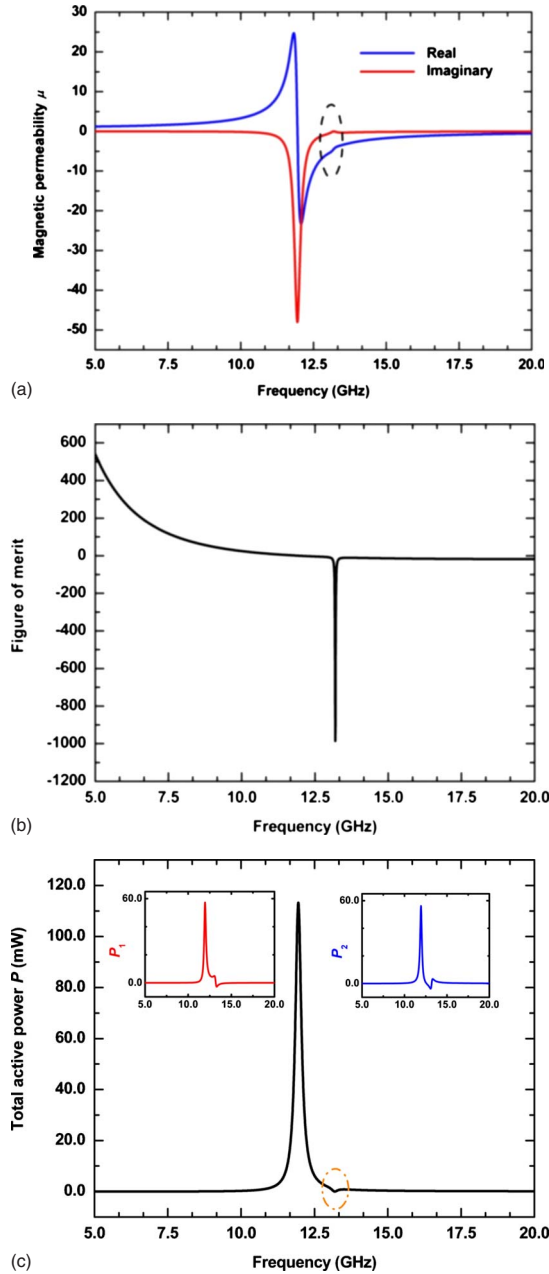


FIG. 4. (Color online) Lossless negative-magnetic metamaterials at GHz frequencies. (a)–(c) report the effective permeabilities and active powers associated with the magnetic metamaterial of Fig. 2. The incident magnetic field has amplitude $H_0=1$ A/m, and the values of the equivalent lumped elements are: $R_1=0.1$ Ω , $R_2=50$ Ω , $C_1=C_2=10$ fF, $C=0.1$ pF, $L_1=L_2=16$ nH. The surfaces of the two meshes are $S_1=S_2=4 \times \pi$ mm² and both are located at the centers of unit cells of volume 25 mm³. Variation with frequency of the: (a) Real and imaginary part of effective μ ; (b) corresponding figure of merit (FOM); (c) total active power $P=P_1+P_2$. The insets illustrate the variation with frequency of the active powers P_1 and P_2 associated with the g-SRR meta-atom 1 and p-SRR meta-atom 2, respectively. Note that there are frequency regions where either P_1 or P_2 become negative, indicating reversal in the sign of the imaginary part of the current circulating in the corresponding SRR particle. In (a) and (c) the highlighted (with a dashed line) regions reveal the regime where the FOM dramatically improves.

Thus, we may have, e.g., assumed that, in addition to the capacitive coupling between the SRR particles, there is also inductive coupling owing to magnetic flux linkage (violation of the “solenoid” approximation). Then, an extra equivalent inductance should have been connected (e.g., in series) to the shunt capacitance C in Fig. 3(b), but (crucially) this would *not* have rendered impossible to reverse the current in the p-SRR meta-atom 2—such a reversal would merely require a suitable adaptation of the particles’ effective lumped-element parameters. It is, also, to be noted that the occurrence of a frequency point where $P_2=0$ and $P_1 \approx 0$ [see insets in Fig. 4(c)] is completely independent of the actual value of $R_1=R_{\text{ohm},1}+R_{\text{rad},1}$ used in the theoretical model, so long as $R_1 \ll R_2$. However, this is not to imply that the distinction between $R_{\text{ohm},1}$ and $R_{\text{rad},1}$ is unnecessary,^{9–11,20–26} first, because $R_{\text{rad},1}$ does make a significant (in fact, dominant) contribution to a metaparticle’s total equivalent resistance, and also because at $f=f_1$ it is the *radiation* (not the intrinsic, ohmic) damping of the g-SRR that is suppressed (for the p-SRR, both, the radiation *and* the ohmic losses are vanishing). Accordingly, at this frequency, the FOM of the magnetic metamaterial rapidly “explodes,” approaching values of ~ 1000 [see Fig. 4(b)]. All importantly, this dramatic improvement in the FOM occurs in a regime where the metamaterial has preserved the negativity in the real part of its effective permeability, i.e., at $f=f_1$ we, indeed, have: $\text{Re}\{\mu\} < 0$.

To further elucidate the mechanism by which each p-SRR avoids dissipating and radiating energy ($P_2=0$) while, simultaneously, helping to suppress the radiation emitted from its neighboring g-SRR, and to corroborate the above two-loop circuit model, we performed three-dimensional, finite-element simulations³⁹ of a suitably designed p-SRR/g-SRR pair of square split rings. Figure 5 reports the absorption spectra for this new SRR arrangement (the p-SRR is shown on the left-hand side in the insets of Fig. 5), as calculated from the full-wave simulations (red line) and the analytic two-loop model (blue line). Note the excellent agreement between the two approaches; in particular, in predicting the *narrowed*-linewidth, abrupt dip in the power absorbed by the metamaterial at $f \approx 3.32$ GHz. The dip is always followed by an *increase* in the absorption at frequencies immediately below *and* above it. Consistently with the two-loop circuit model [see *insets* in Fig. 4(c)], we find from the simulations that there are *two* frequency points where P_2 vanishes:⁴⁰ one ($f \approx 3.20$ GHz; red-line “shoulder” in Fig. 5) where $P_2=0$ and P_1 locally *increases*, and a second one ($f \approx 3.32$ GHz; bottom green dot in Fig. 5) where $P_2=0$ and $P_1 \approx 0$. We note from Fig. 5 that at exactly $f \approx 3.32$ GHz there is no field residing in the p-SRR meta-atom ($P_2=0$), i.e., the lossy p-SRR does *not* contribute at all to the loss-behavior of the metamaterial,⁴⁰ and the intensity of the field localized at the g-SRR meta-atom is small ($P_1 \approx 0$). Moreover, at this frequency, the *currents* in the arms of the g-SRR meta-atoms are found to be *accurately antisymmetric*; thereby, the radiation emitted from one g-SRR arm is *exactly cancelled out* by the radiation emitted from its other arm,^{21,23} resulting in the sharp-linewidth, abrupt dip in the absorption spectra of the metamaterial shown in Fig. 5. Importantly, this enhanced metamaterial loss-behavior occurs in a frequency regime

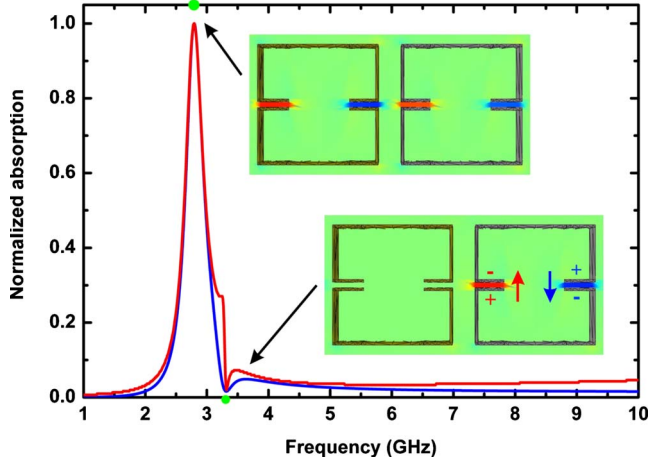


FIG. 5. (Color online) Comparison between the absorption spectra of a metamaterial of the kind shown in Fig. 3(a), as calculated with a finite-element based simulation (red line) and the equivalent analytical two-loop model of Fig. 3(b) (blue line). In the finite-element simulations the square rings had a side length of 4.2 mm, height 0.8 mm, center-to-center distance 5 mm, thickness 0.1 mm, small-arm length 1 mm and a split gap distance of 0.2 mm. The unit-cell size was 50 mm^3 , with periodic boundary conditions applied on its transverse faces. The p-SRR meta-atom 2 (left-hand side in each inset) was simulated using a Drude model with parameters:⁴⁸ $\omega_p = 1.2 \times 10^{16} \text{ rad/s}$ and $\tau = 6.9 \times 10^{-15} \text{ s}^{-1}$, while the g-SRR meta-atom 1 (right-hand side in each inset) had imaginary part of permittivity 500 times smaller than that of the p-SRR. The equivalent lumped-element parameters were: $R_1 = 1.75 \text{ } \Omega$, $R_2 = 55 \text{ } \Omega$, $L_1 = L_2 = 13.5 \text{ nH}$, $C_1 = C_2 = 0.25 \text{ pF}$, $C = 1.1 \text{ pF}$. With the approximate, analytic expressions of refs. 32 and 49, the theoretical values of the equivalent lumped inductances and capacitances would have been: $L_{1,\text{th}} = L_{2,\text{th}} = 13.5 \text{ nH}$ (with the mutual inductance, L_M , subtracted),³² $C_{1,\text{th}} = C_{2,\text{th}} = 0.245 \text{ pF}$ (with the surface capacitance,⁴⁹ as well as the bottom/up and left/right capacitances arising from the proximity of the SRRs in neighboring unit cells, incorporated in the calculation), and $C_{\text{th}} = 11 \text{ pF}$ (where, in addition to the surface capacitance, the “fringing-field” correction⁴⁹ has also been considered). The insets illustrate the spatial distribution of the electric-field component polarized perpendicularly to the gaps of each ring, at the frequencies: 2.79 GHz (absorption maximum) and 3.32 GHz (absorption dip). In the bottom inset, the magnitude of the electric field component has been multiplied by a factor of 4 compared with the top inset. The two arrows in the bottom inset reveal the direction of the induced (antisymmetric) electric dipoles at the two gaps of the g-SRR meta-atom.

(around 3.32 GHz) slightly *above* the main resonance, i.e., in a regime where—similarly to the example studied in Figs. 3 and 4—the permeability of the metamaterial satisfies $\text{Re}\{\mu\} < 0$. Indeed, the extracted^{41,42} real part of the effective permeability for this metamaterial at $f \approx 3.32 \text{ GHz}$ was found to be: $\text{Re}\{\mu\} = -1.86$.

III. ANISOTROPIC MAGNETICALLY ACTIVE METAMATERIAL

A further remarkable property of the g-SRR/p-SRR metamaterial of Fig. 3(a) can be revealed by placing the

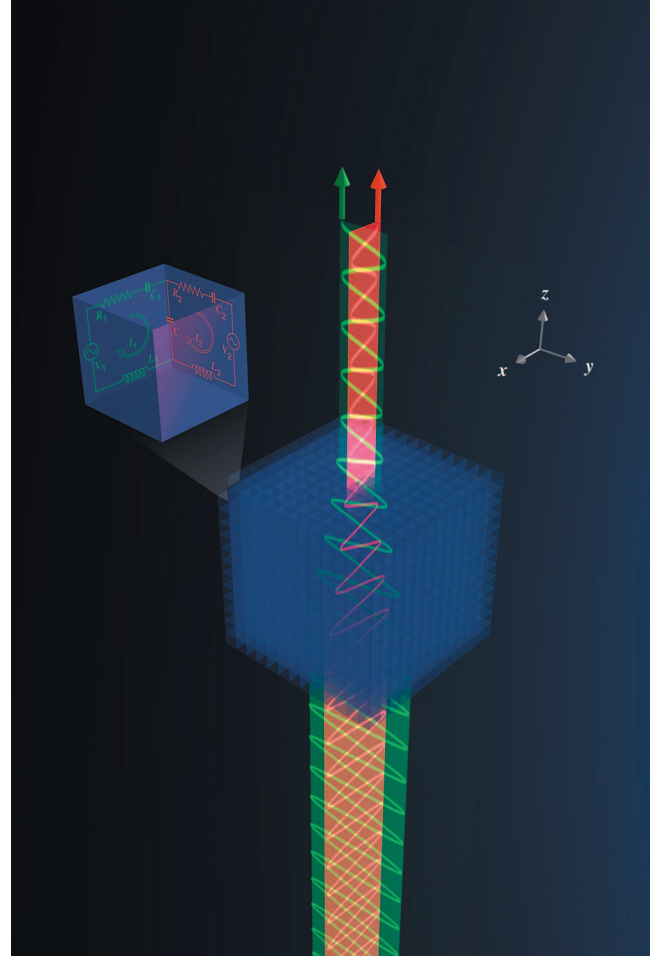


FIG. 6. (Color) Schematic illustration of the anisotropic metamaterial design used for obtaining ‘active’ ($\text{Im}\{\mu\} > 0$) negative-magnetic ($\text{Re}\{\mu\} < 0$) permeabilities. The design is similar to that of Fig. 3(a), but now the two SRR meta-atoms are placed on orthogonal planes. To excite this structure we use a linearly polarized light beam that propagates along the z axis, and has its H_x component (shown in red) oscillating perpendicularly to the p-SRR meta-atom “2,” and its H_y component (shown in green) oscillating perpendicularly to the g-SRR meta-atom 1.

two nonbianisotropic meta-atoms on orthogonal planes, and illuminating the metamaterial by a linearly polarized, monochromatic, plane wave $\mathbf{H} = H_0(\mathbf{x}_0 + \mathbf{y}_0)\exp(i\omega t - i\mathbf{k} \cdot \mathbf{z})$, as illustrated in Fig. 6. Owing to the difference in the conductivities of the two SRR meta-atoms residing on orthogonal planes, this new metamaterial is magnetically anisotropic. Exemplary plots of the elements of the metamaterial’s permeability-matrix are shown in Fig. 7. We find that there are frequency regions where either $\text{Im}\{\mu_x\} > 0$ or $\text{Im}\{\mu_y\} > 0$, i.e., the metamaterial exhibits *active* permeabilities along its crystallographic axes (x and y). Furthermore, this positivity in the imaginary parts of μ_x and μ_y occurs, in both cases, in a regime where the real parts of μ_x and μ_y are *negative* ($\text{Re}\{\mu_x\} < 0$, $\text{Re}\{\mu_y\} < 0$). We stress that in deriving these results (and throughout our present work) we have, similarly to recent reports,⁴³ purposely refrained from deriving conclusions about the imaginary parts of the metamaterials’ effective permeabilities based on reflection/

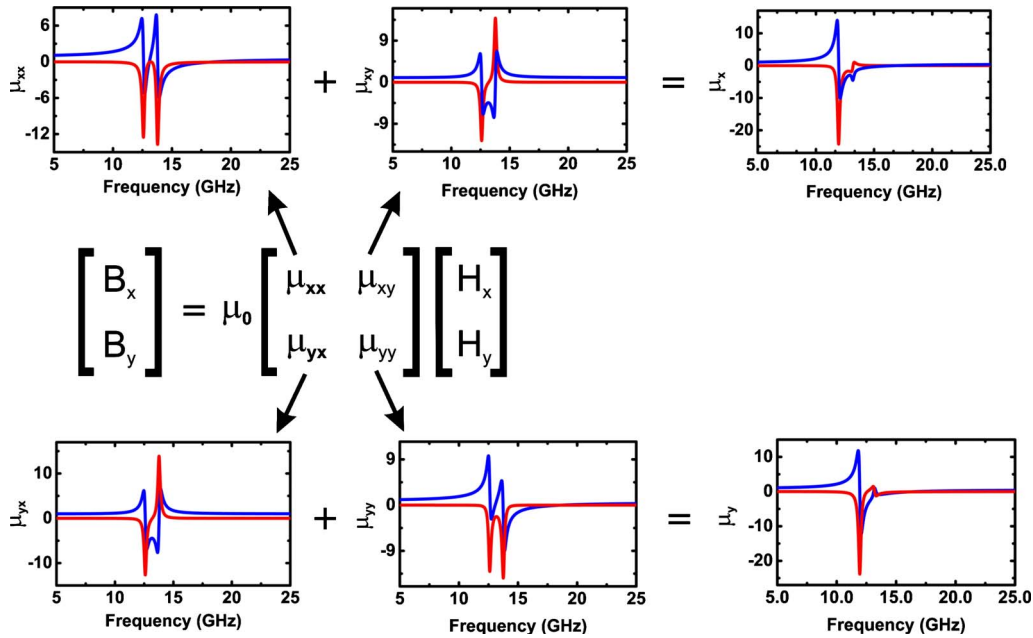


FIG. 7. (Color online) Plots of the elements of the permeability-matrix characterizing the anisotropic metamaterial of Fig. 6. In all calculations we used the electromagnetic and geometric parameters of Figs. 4(a)–4(c). In each plot the blue (red) line corresponds to the real (imaginary) part of the permeability. Note that the diagonal elements are invariably passive ($\text{Im}\{\mu\} < 0$), while the off-diagonal elements exhibit pronounced active imaginary parts ($\text{Im}\{\mu\} > 0$) arising from the exchange of active power between the two coupled RLC resonators (SRR meta-atoms).

transmission methodologies,⁴¹ since such methodologies—unlike the analytic and physically justifiable methodology of, e.g., Ref. 28, which we have herein adopted—may yield unphysical results and/or optimistic figures-of-merit.³⁵ Here, the sound physical origin behind the occurrence of positive $\text{Im}\{\mu_x\}$ and $\text{Im}\{\mu_y\}$ is the *exchange* of active power between the two coupled RLC oscillators of Fig. 6, and the associated *reversal* in the sign of the active powers P_1 and P_2 [see Fig. 4(c)]. Indeed, since the induced emf voltage is (in the frequency domain) purely imaginary ($V_{\text{emf},\ell} = -i\omega\mu_0 S_\ell H_0$, $\ell = 1, 2$), a reversal in the sign of the active power $P_\ell = \text{Re}\{V_\ell I_\ell^*\}$ corresponds to a reversal in the *imaginary* part of the current I_ℓ —and, therefore, to a reversal in the imaginary part of the magnetic permeability associated with that particular meta-atom. Close inspection of $\text{Im}\{\mu_x\}$ and $\text{Im}\{\mu_y\}$ in Fig. 7, indeed shows that these two terms exhibit frequency-variation which is very similar to that of, respectively, P_1 and P_2 in Fig. 4(c). Note that, despite the presence of “active” magnetic permeabilities, the present magnetically anisotropic (nonbianisotropic) metamaterial *does* remain electromagnetically *passive* and does *not* amplify the magnetic or the electric field components propagating inside it. Indeed, in the following section, we present an analysis of the associated eigenproblem based on Maxwell’s equations on a linear basis, from where it is shown that the effective index of the wave propagating inside this medium is given by: $n_{\text{eff}} = (0.5\{\mu_{xx} + \mu_{yy} \pm [(\mu_{xx} - \mu_{yy})^2 + 4\mu_{xy}\mu_{yx}]^{1/2}\})^{1/2}$; hence, it invariably follows that: $\text{Im}\{n_{\text{eff}}\} < 0$. To our knowledge, this is the first instance of a *linear* metamaterial exhibiting a (broadband) active permeability ($\text{Im}\{\mu\} > 0$) in the regime where $\text{Re}\{\mu\} < 0$.

A. Dispersion relations characterizing the magnetically anisotropic metamaterial

As was explained above, the \mathbf{B} - \mathbf{H} constitutive relationship for the magnetically anisotropic medium of Fig. 6 is of the form

$$\begin{bmatrix} B_x \\ B_y \end{bmatrix} = \mu_0 \begin{bmatrix} \mu_{xx} & \mu_{xy} \\ \mu_{yx} & \mu_{yy} \end{bmatrix} \begin{bmatrix} H_x \\ H_y \end{bmatrix}, \quad (2)$$

with a typical plot of the elements of the above permeability-matrix shown in Fig. 7. From that figure one may directly observe that while the diagonal terms remain strictly “passive” ($\text{Im}\{\mu_{xx}\} < 0$, $\text{Im}\{\mu_{yy}\} < 0$) for all frequencies, the off-diagonal terms exhibit pronounced *positive* imaginary parts in certain frequency regions. So large and positive become the terms $\text{Im}\{\mu_{xy}\}$, $\text{Im}\{\mu_{yx}\}$, that the permeabilities $\mu_x = \mu_{xx} + \mu_{xy}$ and $\mu_y = \mu_{yx} + \mu_{yy}$ also exhibit positive (active) imaginary parts in certain (continuous) frequency regions (see Fig. 7). As was mentioned above, this behavior arises from the exchange of active power between the two coupled SRR meta-atoms (RLC oscillators), which results in the *reversal* of the sign of either P_1 or P_2 at some frequencies. Note that the restriction $P_1 + P_2 > 0$ for all frequencies [see Fig. 4(c)], leads to: $\text{Im}\{\mu_{xx}\} + \text{Im}\{\mu_{yy}\} < 0$ for all frequencies, as well—a condition which is, indeed, fulfilled for the permeabilities of Fig. 7.

It is important to note that while the nonbianisotropic (see, also, next sub-section) magnetically anisotropic medium of Fig. 6 does exhibit active permeabilities along its crystallographic axes (x and y), it does *not* (as expected) amplify an electromagnetic wave propagating through it. To

see clearly why, let us assume that the spatiotemporal variation in a uniform, z -propagating, plane wave incident on this medium is of the general form: $\exp(i\omega t - i\beta z)$. Then, from Maxwell's equations ($\mathbf{z}_0 \times \partial_z \mathbf{E} = -i\omega \mathbf{B}$, $\mathbf{z}_0 \times \partial_z \mathbf{H} = -i\omega \mathbf{D}$), we find that for this medium we have

$$\begin{aligned} -i\beta E_x &= -i\omega\mu_0(\mu_{yx}H_x + \mu_{yy}H_y), \\ -i\beta E_y &= -i\omega\mu_0(\mu_{xx}H_x + \mu_{xy}H_y), \\ -i\beta H_x &= -i\omega\varepsilon_0 E_x, \\ -i\beta H_y &= -i\omega\varepsilon_0 E_y. \end{aligned} \quad (3)$$

The above system of equations can be readily solved to determine the effective index, $n_{\text{eff}} = \beta/k_0$, of an eigenwave propagating through the medium

$$n_{\text{eff}}^{\pm} = \left\{ \frac{(\mu_{xx} + \mu_{yy}) \pm [(\mu_{xx} - \mu_{yy})^2 + 4\mu_{yx}\mu_{xy}]^{1/2}}{2} \right\}^{1/2}. \quad (4)$$

An exemplary plot of the variation of n_{eff} with frequency (for the permeabilities of Fig. 7) is shown in Fig. 8. We note that both eigensolutions satisfy: $\text{Im}\{n_{\text{eff}}^{\pm}\} < 0$ (passivity) and: $\text{Re}\{n_{\text{eff}}^{\pm}\} > 0$ (positive effective refractive index). Thus, despite the fact that the metamaterial of Fig. 6 exhibits negative-magnetic active permeabilities and is nonbianisotropic ($\varepsilon = 1 + i0$), both (\pm) eigenwaves propagating inside it experience positive and passive effective refractive indices.

B. Nonbianisotropic design of the 2-DEG magnetically anisotropic metamaterial

In Fig. 9 we are presenting an example of how the magnetically anisotropic structure studied in Fig. 6 can, most straightforwardly, be redesigned such that it is fully nonbianisotropic,^{29,44–46} while maintaining its response that was described in the previous section. Indeed, for $C'_1 = 2C_1$, $C'_2 = 2C_2$, and $C' = 2C$, the magnetic response of the structure of Fig. 9 will be *exactly* the same with that of Fig. 6, but now this new structure will be characterized by an effective electric permittivity $\varepsilon = 1 + i0$ in all directions (electrically isotropic).

Indeed, the charge accumulated in the capacitor $2C_1$ is equal to the charge accumulated to capacitor C'_1 (these two capacitors are connected in series), but the dipole moments generated in these two capacitors are *oppositely* directed (and of the same magnitude if the separation of the capacitors' plates is the same for both capacitors); hence, they infallibly cancel out each other. The same, of course, also holds true for the capacitor pairs $\{2C_2 \text{ and } C'_2\}$ and $\{2C \text{ and } C'\}$.⁴⁷ Note, also, that in the structure of Fig. 9, even the dipole moments generated (along diagonal directions) by neighboring capacitors (e.g., C'_1 and C' , etc) mutually cancel. This structure is, thus, in every sense a fully *nonbianisotropic* one, characterized by an effective permittivity $\varepsilon = 1 + i0$ in all directions.

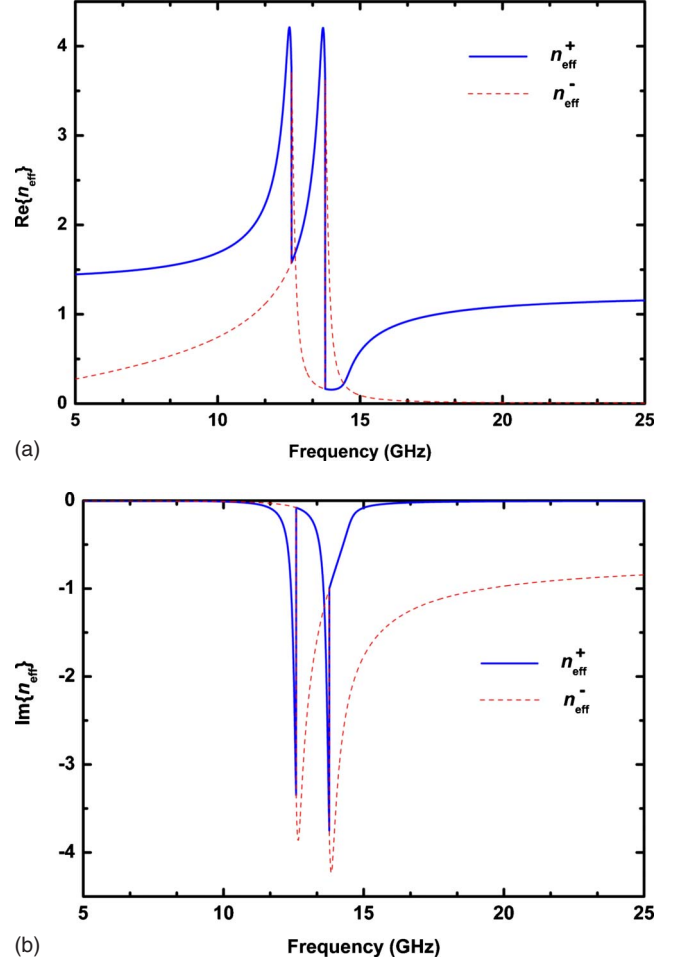


FIG. 8. (Color online) (a) Real and (b) imaginary part of the effective refractive index of the eigenwave(s) propagating through the metamaterial of Fig. 6.

IV. ROBUSTNESS TO DISSIPATIVE LOSSES AND EXTENSION TO THE OPTICAL REGIME

It turns out that the underlying mechanism (i.e., the exchange of active power between the p-SRR/g-SRR meta-atoms) that is responsible for enabling the suppression of radiation damping in the metamaterial designs of Figs. 3–5 and the appearance of active permeabilities in the metamate-

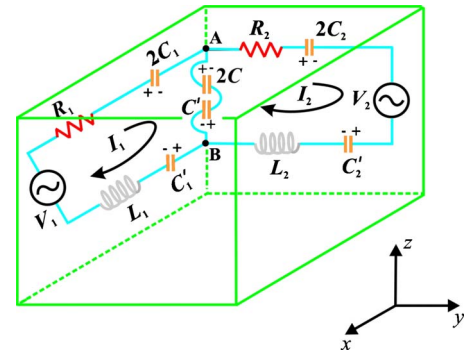


FIG. 9. (Color online) Nonbianisotropic implementation of the configuration shown in Fig. 6.

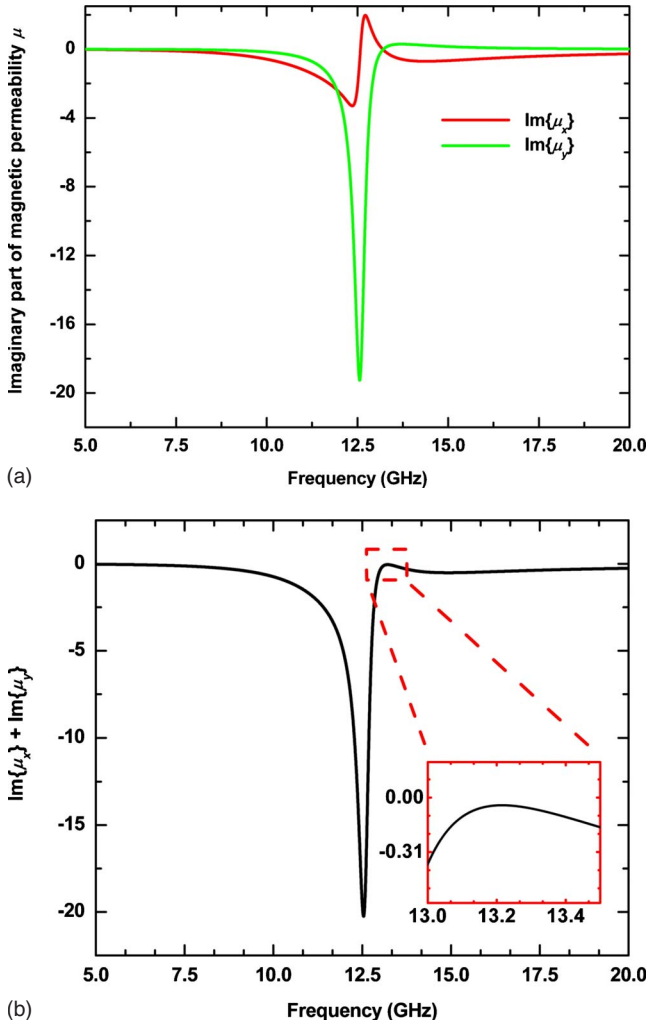


FIG. 10. (Color online) (a) Imaginary parts of μ_x and μ_y for a metamaterial with electromagnetic and geometric parameters similar to those used in Fig. 4, but now with $R_1=1 \Omega$ and $R_2=500 \Omega$. (b) Sum of the imaginary parts of μ_x and μ_y .

rial of Fig. 6, is extremely resilient and robust to the presence of ohmic losses, insofar as the *difference* in (*not the actual values of*) the ohmic resistances of the meta-atoms is substantial.

Indeed, from Fig. 10 one observes that even when the ohmic resistances in each meta-atom increases by an order of magnitude compared with those of Fig. 4(i).e., for new resistances: $R_1=1 \Omega$, $R_2=500 \Omega$, which are typical values for the overall equivalent resistances of individual SRR meta-atoms in the optical regime,⁹ there are, as before, regions wherein the imaginary parts of the effective permeabilities become positive—and with: $\text{Im}\{\mu_1\} + \text{Im}\{\mu_2\} < 0$ for every frequency; see Fig. 10(b). The same holds true for *any* increase in R_1 and R_2 , to the extent that we do not enter the “overdamped” region wherein there is no effective magnetic oscillation (response) in the metamaterial at all. Ultimately, this robustness against losses is, as highlighted before, owing to the fact that the underlying mechanism relies critically on an *imbalance* in the values of the ohmic resistances of the pair of the geometrically identical meta-atoms, and *not* on the actual values of the resistances themselves. As long as

such an imbalance is present (and provided that we are not in the overdamped regime) there will always be power flowing *away* from one meta-atom (RLC oscillator) toward its partner, and reversing the current circulating in this second meta-atom. This will result in algebraically negative active power associated with the meta-atom whose current has been reversed, and in *positive* (active) imaginary part for the corresponding magnetic susceptibility/permeability.

V. CONCLUSIONS

In summary, we have presented a design that, up to THz frequencies, allows for constructing practically “lossless” negative-magnetic metamaterials. The blueprint is based on a two-degrees-of-freedom (2-DEG) topology wherein poor-conductor SRR (p-SRR) meta-atoms manage to suppress the radiation damping associated with each existing good-conductor g-SRR meta-atom of a magnetic metamaterial, *without* inserting additional (radiation or ohmic) losses into the system—and in a regime where the metamaterial’s effective permittivity is negative. We have, further, shown that placing the two SRR meta-atoms on orthogonal planes results in a magnetically anisotropic metamaterial exhibiting (broadband) active permeabilities along its principal crystallographic axes. Both of the above features (suppression of radiation losses in the regime where $\text{Re}\{\mu\} < 0$, and active permeabilities) rely solely on the difference in (*not* the actual values of) the ohmic resistances of the SRR meta-atoms; hence, they are extendable to the optical regime. Given the simplicity of the herein reported designs and the availability of mature metamaterial-growth technologies, it is believed that these recipes may conceivably lead to designs for ultralow-loss or magnetically active negative-permeability metamaterials to be used in a wealth of exciting and useful applications.^{1-8,15,27}

ACKNOWLEDGMENTS

We thank D. P. Aryal for discussions and Z. Davies for help with the preparation of the supplementary material Documents No. 1 and 2. This work was supported by the UK Engineering and Physical Sciences Research Council (EPSRC). K.L.T. acknowledges support by the Royal Academy of Engineering and the EPSRC. M.S.W. would like to acknowledge financial support provided by the Natural Science and Engineering Research Council of Canada (NSERC).

APPENDIX: REMARKS ON ACTIVE AND REACTIVE POWERS

Consider two circuits, C_1 and C_2 , electrically connected with two conducting wires, as shown in Fig. 11. Circuit C_1 contains an ideal source and passive elements (resistors, inductors, capacitors), while circuit C_2 contains only passive elements. Let us assume that the time-domain voltage, $V(t)$, and the current, $I(t)$, shown in Fig. 11, are sinusoidal functions of time, i.e.: $V(t) = V_0 \cos(\omega t)$, and $I(t) = I_0 \cos(\omega t - \varphi)$, where φ is the phase difference between the current and the voltage. For the sign convention shown in Fig. 11, a positive

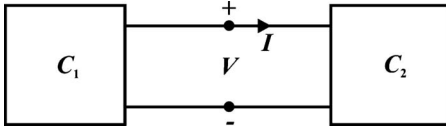


FIG. 11. Schematic illustration of two electrically connected circuits.

time-domain (instant) power, $P(t)=V(t)I(t)>0$, means that *electrical power flows from circuit C_1 toward circuit C_2* . Conversely, if $P(t)<0$ then *power flows from circuit C_2 to circuit C_1* .

If circuit C_1 contains only an (ideal) source, we always have: $P(t)>0$ (power flows *away* from the source). It is, then, instructive to write the expression for the instant power $P(t)$ in the form

$$P(t) = V_{\text{rms}}I_{\text{rms}} \cos \varphi [1 + \cos(2\omega t)] + V_{\text{rms}}I_{\text{rms}} \sin \varphi \sin(2\omega t), \quad (\text{A1})$$

where $V_{\text{rms}}=V_0/\sqrt{2}$ and $I_{\text{rms}}=I_0/\sqrt{2}$. Since we have assumed that the circuit C_2 contains only passive elements, the phase difference φ between the current and the voltage will be: $-\pi/2 < \varphi < \pi/2$, and therefore the first term on the RHS of Eq. (A1) will be positive, corresponding to power flowing from circuit C_1 to circuit C_2 , where it is consumed (dissipated). For this reason, this power, $P_R(t)=V_{\text{rms}}I_{\text{rms}} \cos \varphi [1 + \cos(2\omega t)]$, is called real or active power. The active power varies between 0 and $2V_{\text{rms}}I_{\text{rms}} \cos \varphi$ in one period, and a metric that is frequently used for it, is its time-averaged value: $\bar{P}=V_{\text{rms}}I_{\text{rms}} \cos \varphi$, which customarily is again referred to as active power. By contrast, the second term in the right-hand side of Eq. (A1), $P_x(t)=V_{\text{rms}}I_{\text{rms}}(\sin \varphi)\sin(2\omega t)$, changes sign twice during the period $T=2\pi/\omega$. During the first half-period, P_x flows from C_1 to C_2 , while in the second half-period the direction of the flow of P_x is reversed, i.e., P_x now flows from C_2 to C_1 , so that the overall effect is zero.

Because of the fact that P_x does not (on average) produce any work, it is usually referred to as *reactive power*. Since the time-averaged value of P_x is zero, a metric that is frequently used for its quantification is its *amplitude*, $Q = V_{\text{rms}}I_{\text{rms}} \sin \varphi$. Generally, the reactive power refers to the part of the instant power $P(t)$ that is sent by a source to the inductors and capacitors of the circuit, stored there temporarily, and then sent back to the source.

Considering the frequency-domain complex power, S

$$S = \tilde{V}\tilde{I}^* = V_{\text{rms}}I_{\text{rms}}e^{i(\theta_1-\theta_2)} = V_{\text{rms}}I_{\text{rms}}e^{i\phi}. \quad (\text{A2})$$

with $\tilde{V}=V_{\text{rms}}e^{i\theta_1}$, $\tilde{I}=I_{\text{rms}}e^{i\theta_2}$, and θ_1, θ_2 being the angles of the rotating vectors \tilde{V} and \tilde{I} with the real axis, it can be readily seen that the reactive power is given by: $Q=\text{Im}\{S\}$, while the (time-averaged) active power is given by: $\bar{P}=\text{Re}\{S\}$, which is the relation that we used in the calculations of the active powers referred to in the main text.

It should be noted that when the circuit C_2 does *not* contain sources (and C_1 contains only an ideal source), the active power \bar{P}_1 in C_1 is strictly positive, i.e., C_1 only *remits* real power to (does *not* receive real power from) C_2 wherein it is converted into heat at the resistances. In contrast, if C_2 also includes sources of electrical energy, then it is possible that \bar{P}_1 may become negative (for the sign convention shown in Fig. 11) in a frequency region, corresponding to active power being received by C_1 , i.e., in that region C_1 acts as a *load*: it does not remit real power to C_2 , but *receives* active power from the neighboring meshes (in this case, C_2) that it is electrically connected with. Note, however, that the total active power, $P_{\text{tot}}=\sum_i P_i$ ($i=1, \dots, n$), n being the total number of electrically connected meshes, must still be positive *at every frequency point*, since overall we have a net consumption of real power. These features are, indeed, precisely what we observed in the analytic calculations of the active powers that were reported in Fig. 4(c) in the main body of this work.

*Author to whom correspondence should be addressed; o.hess@surrey.ac.uk; <http://www.ati.surrey.ac.uk/tac/home>

¹M. C. K. Wiltshire, J. B. Pendry, I. R. Young, D. J. Larkman, D. J. Gilderdale, and J. V. Hajnal, *Science* **291**, 849 (2001).

²C. Enkrich, M. Wegener, S. Linden, S. Burger, L. Zschiedrich, F. Schmidt, J. F. Zhou, Th. Koschny, and C. M. Soukoulis, *Phys. Rev. Lett.* **95**, 203901 (2005).

³J. B. Pendry, *Phys. Rev. Lett.* **85**, 3966 (2000).

⁴J. B. Pendry, D. Schurig, and D. R. Smith, *Science* **312**, 1780 (2006).

⁵N. Engheta, *Science* **317**, 1698 (2007).

⁶K. L. Tsakmakidis, A. D. Boardman, and O. Hess, *Nature (London)* **450**, 397 (2007).

⁷V. G. Veselago, *Sov. Phys. Usp.* **10**, 509 (1968).

⁸C. M. Soukoulis, J. Zhou, Th. Koschny, M. Kafesaki, and E. Economou, *J. Phys.: Condens. Matter* **20**, 304217 (2008).

⁹M. Husnik, M. W. Klein, N. Feth, M. König, J. Niegermann, K. Busch, S. Linden, and M. Wegener, *Nat. Photonics* **2**, 614

(2008).

¹⁰T. P. Meyrath, T. Zentgraf, and H. Giessen, *Phys. Rev. B* **75**, 205102 (2007).

¹¹B. Sauviac, C. R. Simovski, and S. A. Tretyakov, *Electromagnetics* **24**, 317 (2004).

¹²R.-L. Chern and Y.-T. Chen, *Phys. Rev. B* **80**, 075118 (2009).

¹³S. A. Maier, *Plasmonics: Fundamentals and Applications* (Springer, New York, 2007).

¹⁴A. P. Hibbins, E. Hendry, M. J. Lockyear, and J. R. Sambles, *Opt. Express* **16**, 20441 (2008).

¹⁵V. M. Shalaev, *Nat. Photonics* **1**, 41 (2007).

¹⁶S. A. Ramakrishna and J. B. Pendry, *Phys. Rev. B* **67**, 201101 (2003).

¹⁷B. Nistad and J. Skaar, *Phys. Rev. E* **78**, 036603 (2008).

¹⁸J. B. Pendry, *Science* **322**, 71 (2008).

¹⁹D. D. Smith, H. Chang, K. A. Fuller, A. T. Rosenberger, and R. W. Boyd, *Phys. Rev. A* **69**, 063804 (2004).

²⁰S. Zhang, D. A. Genov, Y. Wang, M. Liu, and X. Zhang, *Phys.*

- Rev. Lett.* **101**, 047401 (2008).
- ²¹N. Papasimakis, V. A. Fedotov, and N. I. Zheludev, *Phys. Rev. Lett.* **101**, 253903 (2008).
- ²²P. Tassin, L. Zhang, Th. Koschny, E. N. Economou, and C. M. Soukoulis, *Phys. Rev. Lett.* **102**, 053901 (2009).
- ²³N. Liu, L. Langguth, Th. Weiss, J. Kästel, M. Fleischhauer, T. Pfau, and H. Giessen, *Nat. Mater.* **8**, 758 (2009).
- ²⁴C.-Y. Chen, I.-W. Un, N.-H. Tai, and T.-J. Yen, *Opt. Express* **17**, 15372 (2009).
- ²⁵T. Q. Li, H. Liu, T. Li, S. M. Wang, J. X. Cao, Z. H. Zhu, Z. G. Dong, S. N. Zhu, and X. Zhang, *Phys. Rev. B* **80**, 115113 (2009).
- ²⁶R. Singh, C. Rockstuhl, F. Lederer, and W. Zhang, *Phys. Rev. B* **79**, 085111 (2009).
- ²⁷J. B. Pendry, *Nature (London)* **460**, 579 (2009).
- ²⁸J. B. Pendry, A. J. Holden, D. J. Robbins, and W. J. Stewart, *IEEE Trans. Microwave Theory Tech.* **47**, 2075 (1999).
- ²⁹J. D. Baena, L. Jelinek, and R. Marqués, *Phys. Rev. B* **76**, 245115 (2007).
- ³⁰M. Gorkunov, M. Lapine, E. Shamonina, and K. H. Ringhofer, *Eur. Phys. J. B* **28**, 263 (2002).
- ³¹A. Ishikawa, T. Tanaka, and S. Kawata, *Phys. Rev. Lett.* **95**, 237401 (2005).
- ³²H. Chen, L. Ran, J. Huanfu, T. M. Gregorczyk, and J. A. Kong, *J. Appl. Phys.* **100**, 024915 (2006).
- ³³M. Kafesaki, I. Tsiapa, N. Katsarakis, Th. Koschny, C. M. Soukoulis, and E. N. Economou, *Phys. Rev. B* **75**, 235114 (2007).
- ³⁴N.-H. Shen, G. Kenanakis, M. Kafesaki, N. Katsarakis, E. N. Economou, and C. M. Soukoulis, *J. Opt. Soc. Am. B* **26**, B61 (2009).
- ³⁵Th. Koschny, P. Markoš, E. N. Economou, D. R. Smith, D. C. Vier, and C. M. Soukoulis, *Phys. Rev. B* **71**, 245105 (2005).
- ³⁶J. E. Sipe and J. Van Kranendonk, *Phys. Rev. A* **9**, 1806 (1974).
- ³⁷S. Ramo, J. R. Whinnery, and T. Van Duzer, *Fields and Waves in Communication Electronics* (Wiley, New York, 1994), p. 206.
- ³⁸In a sense, the lossy p-SRR meta-atom 2 may serve as a local probe of the field (re-) emitted by its neighboring g-SRR meta-atom 1. If the p-SRR meta-atom remains unexcited, this is an indication that the g-SRR does not radiate. See, also, Ref. 23.
- ³⁹JCMwave GmbH, www.jcmwave.com.
- ⁴⁰See supplementary material at <http://link.aps.org/supplemental/10.1103/PhysRevB.81.195128> for 1) a QuickTime movie illustrating the evolution of the spatial distribution (at a constant plane, cutting the SRRs in the middle of their height) of the electric field component (polarized perpendicularly to the small, horizontal arms of the rings) for frequencies ranging from 2.6 GHz to 3.7 GHz. Note that there are *two* frequency points (3.30 GHz and 3.32 GHz) where the field in the left p-SRR meta-atom 2 vanishes. 2) A QuickTime movie illustrating the spatial distribution of the electric field component at successive planes inside a unit cell of the three-dimensional metamaterial studied in Fig. 5. The frequency at which the displayed results were obtained is $f=3.32$ GHz, corresponding to the dip (see Fig. 5) in the absorption spectra of the magnetic metamaterial.
- ⁴¹D. R. Smith, S. Schultz, P. Markoš, and C. M. Soukoulis, *Phys. Rev. B* **65**, 195104 (2002).
- ⁴²J. J. H. Cook, K. L. Tsakmakidis, and O. Hess, *J. Opt. A, Pure Appl. Opt.* **11**, 114026 (2009).
- ⁴³J. K. Gansel, M. Thiel, M. S. Rill, M. Decker, K. Bade, V. Saile, G. von Freymann, S. Linden, and M. Wegener, *Science* **325**, 1513 (2009).
- ⁴⁴J. García-García, F. Martin, J. D. Baena, R. Marqués, and L. Jelinek, *J. Appl. Phys.* **98**, 033103 (2005).
- ⁴⁵R. Marqués, F. Medina, and R. Rachid-El-Idrissi, *Phys. Rev. B* **65**, 144440 (2002).
- ⁴⁶J. D. Baena, J. Bonache, F. Martin, R. M. Sillero, F. Falcone, T. Lopetegui, M. A. G. Laso, J. García-García, I. Gil, M. F. Portillo, and M. Sorolla, *IEEE Trans. Microwave Theory Tech.* **53**, 1451 (2005).
- ⁴⁷In Fig. 9, we have assumed that $I_1 > I_2$, so that current (of positive carriers) flows downwards, from point A to point B; if $I_1 < I_2$, then the polarity of the capacitors $2C$ and C' will be reversed, without affecting any of the mentioned conclusions.
- ⁴⁸P. B. Johnson and R. W. Christy, *Phys. Rev. B* **6**, 4370 (1972).
- ⁴⁹O. Sydoruk, E. Tatartschuk, E. Shamonina, and L. Solymar, *J. Appl. Phys.* **105**, 014903 (2009).